The role of duty cycle of substrate pulse biasing in the deposition of amorphous carbon ultrathin films by filtered cathodic vacuum arc

J. Xie and K. Komvopoulos*

Department of Mechanical Engineering, University of California, Berkeley, CA 94720, USA

Abstract

The effect of the duty cycle of substrate pulse biasing on the structure (hybridization), composition, thickness, residual stress, and surface roughness of ultrathin amorphous carbon (*a*-C) films synthesized by filtered cathodic vacuum arc was examined in the light of high-resolution transmission electron microscopy, cross-sectional electron energy loss spectroscopy, Raman spectroscopy, residual stress measurements, atomic force microscopy. The through-thickness structure and elemental composition reveal a multilayer film structure consisting of an interface layer of C and Si, a buffer layer of varying sp^3 fraction and relatively constant C concentration, a bulk-film layer of constant sp^3 concentration, and a surface layer rich in sp^2 hybridization. It is shown that a 65% duty cycle yields the smoothest and thinnest *a*-C films with relatively high sp^3 content, whereas a 75% duty cycles produces relatively thicker and rougher *a*-C films with maximum sp^3 carbon concentration and highest residual (compressive) stress. The results of this study have direct implications in ultrahigh-density magnetic recording, where very smooth ultrathin *a*-C films with high sp^3 contents are of critical importance to the longevity and reliability of hard-disk drives.

Index Terms – Amorphous carbon, duty cycle, filtered cathodic vacuum arc, head-disk interface, hybridization, pulse biasing, residual stress, surface roughness, ultrathin films

*Corresponding author:
Tel.: 510-642-2563, Fax: 510-642-5539, E-mail: kyriakos@me.berkeley.edu (K. Komvopoulos)

Submitted to *IEEE Transactions on Magnetics*.

I. INTRODUCTION

Amorphous carbon (*a*-C) films are extensively used as protective overcoats in various cutting-edge technologies, such as hard-disk drives (HDDs) and microelectromechanical systems, mainly because of their high hardness and excellent wear and corrosion resistance [1–3]. In HDDs, information is stored in the magnetic medium of a hard disk by the magnetic field applied by a transducer embedded into the trailing edge of a magnetic head flying in close proximity with the spinning hard disk. To protect the head-disk interface from damage due to intermittent asperity contact and corrosion, the magnetic head and hard-disk surfaces are coated with a continuous, smooth, ultrathin *a*-C film [4,5]. The structure of the *a*-C overcoat is characterized by the dominant type of atomic carbon bonding, i.e., sp^2 (graphite-like) and sp^3 (diamond-like) carbon atom hybridization. A high *a*-C film hardness usually correlates with good film properties [6,7], which strongly depend on sp^3 concentration. Because the data storage density in HDDs exhibits an exponential increase with decreasing distance between the magnetic medium and the read-write element of the magnetic head [8], the thickness of the protective *a*-C film has been dramatically reduced in recent HDDs; for example, current demands for ultrahigh storage capacity necessitate a carbon overcoat thickness of ~2–3 nm [9–14]. The significantly reduced overcoat thickness in next-generation HDDs raises serious concerns about the uniformity, structure, roughness, mechanical/tribological properties, and corrosion resistance of the carbon overcoat. For example, traditional physical vapor deposition methods (e.g., sputtering) cannot produce continuous *a*-C films of thickness less than 5 nm. Currently, filtered cathodic vacuum arc (FCVA) is the only demonstrated method that can produce hydrogen-free *a*-C films of thickness ~1–3 nm with high sp^3 contents, good mechanical properties, and high wear resistance [14,15].

Increasing demands for HDDs with even higher storage densities (i.e., >10 Tbit/in^2) [16–18] have motivated the development of new information storage technologies which are not limited by the superparamagnetic effect, such as heat-assisted magnetic recording (HAMR) [4]. The HAMR technology relies on a laser-optical system integrated into the magnetic head to locally heat a fine-grained magnetic medium possessing high magnetic anisotropy energy density above its Curie temperature to effectively

store information in single bits. However, repetitive localized laser heating may destabilize the structure of the carbon overcoat of HAMR hard disks [19,20]. Thus, the structural stability of the *a*-C overcoat is an additional critical requirement in HAMR technology. Recent studies have shown that FCVA-synthesized *a*-C films exhibit superior thermal stability under intense and rapid thermal heating and cooling conditions [21]; therefore, these films are strong candidates for protective overcoats in HAMR HDDs. The high thermal stability of *a*-C films deposited by FCVA is characteristic of a predominantly sp^3-hybridized structure. In FCVA, the film precursors are energetic C^+ ions as opposed to atoms and/or clusters of atoms in traditional physical and chemical vapor deposition methods. Thus, depending on the FCVA deposition conditions (e.g., pulsed bias voltage), C^+ ion bombardment of the substrate surface results in deposition alternating with direct and recoil implantation. Because of the high-quality plasmas generated by FCVA, the ion bombardment energy can be easily modulated by applying a pulsed bias voltage to the substrate. Consequently, C^+ ion acceleration through the plasma sheath during substrate biasing produces intense ion bombardment onto the growing film surface and, in turn, direct and recoil implantation, whereas when the substrate bias is off, the low ion kinetic energy promotes ion-atom and atom-atom collision cascades and atom diffusion occur at the film surface, predominantly resulting in the deposition of film material.

Although decreasing the deposition time and/or arc discharge current reduce the total number of ions arriving at the growing film surface and, hence, the film thickness, both of these approaches are limited because arcing at the cathode surface cannot be stabilized within a very short deposition time (e.g., <5 s) and there is a minimum arc discharge current for igniting the plasma. A more effective method to reduce the film thickness is to increase the ion bombarding energy. High-energy ions can sputter off atoms from the film surface, producing thinner films compared to less energetic ions [22]. However, the film structure and physical properties are strong functions of the ion energy. For example, high C^+ ion energy intensifies the collisions between incoming carbon ions and surface atoms, which is conducive to sp^3 hybridization. However, high C^+ ion energy may also promote thermal relaxation, which favors sp^2 hybridization and sp^3-to-sp^2 re-hybridization. Because of these competing processes, there is an optimum

C^+ ion energy (typically, ~120 eV) for depositing *a*-C films of high sp^3 content [3,23]. Furthermore, changes in ion energy could be detrimental to the film properties [3,24–26]. Adjusting the incidence angle of bombarding ions and/or duty cycle of the pulsed substrate bias are more desirable for controlling the film thickness and properties, because their effect on the film structure and properties is secondary compared to the ion energy. While the effect of the incidence angle of impinging ions on the roughness and structure of FCVA-synthesized *a*-C films has been examined in a previous study [27], a comprehensive study of the effect of the duty cycle of the pulsed substrate bias on the quality of *a*-C films has not been reported yet.

There are mainly two advantages of substrate pulse biasing compared to dc substrate biasing of the substrate. First, the surface potential of a non-conductive film can be controlled by applying a pulsed bias voltage, whereas dc biasing leads to surface charging that produces a surface potential significantly different than the applied bias voltage [28]. Second, substrate pulse biasing enables the variation of the duty cycle of the pulsed bias voltage, defined as the ratio of the time that the bias voltage is applied to the pulsed bias period, and alternating between ion bombardment and deposition can significantly affect both the film properties and film/substrate interface characteristics. A negative substrate bias voltage accelerates the C^+ ions traveling through the plasma sheath, and the increase of the C^+ ion kinetic energy promotes ion sputter etching of weakly bonded carbon atoms and direct/recoil implantation. Alternatively, in the absence of substrate biasing, the low C^+ ion energy (~20 eV) mainly favors atomic surface diffusion and, thus, film growth is the dominant deposition process. Hence, different contributions of the sputtering/bombardment and deposition processes to film synthesis may be achieved by varying the duty cycle of the pulsed bias voltage, thereby affecting the film structure and properties.

The dependence of the growth and properties of films deposited by sputtering [28], ion plating [29], plasma immersion ion implantation [30], plasma-enhanced chemical vapor deposition [31], and FCVA including substrate pulse biasing [32] on the duty cycle has attracted significant attention. For example, Anders et al. [32] deposited diamondlike carbon films of thickness between 70 and 100 nm by pulsed bias cathodic vacuum arc and reported that a 50% duty cycle and –100 V pulsed bias voltage

produced ~100-nm-thick films with the highest hardness; however, the effect of duty cycle in the range of 50–100% on the film thickness was not examined. Sheeja et al. [33] studied the effects of the pulsed bias period on the growth rate, microstructure, and mechanical behavior of 70–130-nm-thick *a*-C films deposited by FCVA for a bias voltage of –80 V and reported a minimum film stress for 0.125% duty cycle and smooth and hard films for a duty cycle in the range of 0.03–3.0%; however, microanalysis results of the film structure were not obtained. XPS studies of Wu et al. [34] reported that diamondlike carbon films deposited by pulsed bias cathodic vacuum arc possessed the highest sp^3 content (50.8%) and hardness (49 GPa) for 12.5% duty cycle; however, the effect of a higher duty cycle on the film structure and properties was not examined and detailed cross-sectional characterization was not performed.

According to the subplantation model [35], the intensification of energetic C^+ ion bombardment due to substrate pulse biasing leads to the formation of a three-layer film structure consisting of interface layer, bulk film, and surface layer [26,36–38]. Therefore, the properties of ultrathin films deposited by the FCVA method are expected to differ from those of thick films due to the greater contributions of the interface and surface layers to the bulk film properties. Despite valuable information about the effect of substrate pulse biasing on carbon film growth derived from the previous studies, the reported results are either for relatively thick films (>30 nm) or insight into the duty cycle effect on the through-thickness structure is limited. Therefore, an in-depth investigation of the effect of duty cycle of substrate pulse biasing on the structure, composition, and physical properties of FCVA-synthesized *a*-C films is of paramount importance.

The objective of this study is to elucidate the effect of the duty cycle of substrate pulse biasing on the through-thickness structure and composition, thickness, residual stress, and surface roughness of FCVA-synthesized ultrathin *a*-C films. The surface topography and through-thickness structure of the synthesized films were examined by atomic force microscopy (AFM) and high-resolution transmission electron microscopy (HRTEM), respectively, whereas the overall and cross-sectional elemental film structure was examined by analytical Raman spectroscopy and electron energy loss spectroscopy (EELS), respectively, and the average film stress was calculated by the curvature method. Results are contrasted to

elucidate the effects of the duty cycle of substrate biasing on the quality of ultrathin *a*-C films, to determine the optimum duty cycle for FCVA film deposition, and to provide insight into the minimum thickness of *a*-C films that can be achieved under optimum substrate bias conditions.

II. EXPERIMENTAL PROCEDURES

A. Film Synthesis

Silicon substrates (10×10 mm^2) cut from commercially available p-type Si(100) wafers were cleaned by rinsing in acetone and isopropanol for 10 min, respectively, before coating them with ultrathin *a*-C films in a custom-made FCVA system [22,25]. Briefly, film synthesis comprised pumping down the vacuum chamber to a low base pressure ($<5 \times 10^{-7}$ Torr) to remove any residual gases adsorbed onto the chamber walls; introducing Ar gas into the chamber that increased the working pressure to 2×10^{-4} Torr; sputter etching the Si substrate for 2 min with 500-eV Ar^+ ions of 60° incidence angle (measured from the normal to the substrate surface) generated by a 64-mm Kaufman ion source to remove the native SiO_2 layer; and, after reaching a base pressure of $<5 \times 10^{-7}$ Torr, inducing plasma arcing at the cathode (99.99% pure graphite) surface with a mechanical striker. The plasma was stabilized by applying to the cathode a cusp-configuration magnetic field [22]. Any macroparticles and/or droplets ejected from the cathode were filtered out by the magnetic field generated by out-of-plane S-shape electromagnetic coils. The current of the auxiliary, upstream, and downstream coils was set at 30.5, 30.9, 29.6 A, respectively. Under these current plasma conditions, only high-purity (~99.99%) C^+ ions were produced at the filter exit. In all film depositions, the incidence ion angle was fixed at 90° (i.e., ion impingement normal to the substrate surface) and the deposition time was set at 30 s. To control the C^+ ion energy during film deposition, an optimum pulsed bias voltage of –100 V [3,23,25,32] was applied to the substrate holder. To enhance the film uniformity in the radical direction, the substrate was rotated at 60 rpm during processing.

B. Microanalysis Methods

Cross-sectional HRTEM samples were prepared by mechanical grinding, dimpling, and surface finishing by ion milling. To distinguish the *a*-C film from the epoxy glue and to ensure that the EELS carbon signal was only due to the *a*-C film, a thin Au capping layer was sputtered onto the surface before sample bonding. The film samples were first cleaved into two halves and glued face-to-face with M-bond 610 epoxy. After curing at 160°C for 1.5 h, additional Si(100) was glued to both sides of the sandwiched film samples to increase the sample thickness greater than 3 mm. Then, the samples were sectioned into ~500-μm-thick slices with a diamond blade and saw-cut to 3-mm-diameter disks. Finally, the disks were ground down to a thickness of <20 μm at the center by double-side dimpling and then ion milled from the top and the bottom with Ar^+ ion guns (PIPS II, Gatan) operated at 4.5 kV. A 5° incidence Ar^+ ion angle was used to produce a through-thickness hole across the sample/epoxy/sample interface. More details about the TEM sample preparation method used in this study can be found elsewhere [39].

HRTEM images and EELS spectra were obtained with a FEI Tecnai (F20 UT) microscope operated at 200 kV, using a CCD camera (2048 × 2048 pixels) positioned 42 mm behind the Gatan imaging filter. A 13.5-mrad C2 semi-angle and a 100-μm C2 aperture were used in the present study. The EELS collection semi-angle was set at 47 mrad. Using the full width at half maximum of the zero-loss peak, the energy resolution was found to be equal to 0.58 eV, which is sufficiently low for distinguishing sp^2 from sp^3 hybridizations, considering that the band gap difference between sp^2 and sp^3 is about 0.8–0.9 eV. The spatial resolution of the scanning TEM (STEM) without a monochromator was 0.14 nm.

The film structure was further examined with a visible Raman spectroscope (WiRE, Renishaw Raman Imaging Microscope), which uses a 514.5-nm Ar^+ ion laser that can be focused to a spot of <4 μm in diameter. Raman spectra were recorded in the range of 850–1950 cm^{-1}. After background noise subtraction, the spectra were deconvoluted by fitting two Gaussian distributions corresponding to the *D* and *G* peaks, associated with the in-plane bond stretching vibration mode of the sp^2 bonds and the breathing mode of the sp^2 bonds in the aromatic rings, respectively [3]. For statistical analysis, Raman spectra were collected from at least three different locations on each film surface.

C. Surface Roughness and Film Thickness Measurement

The film surface roughness was determined from 2 × 2 μm^2 images acquired with an AFM (NanoScope II, Digital Instruments) operated in the tapping mode. All AFM images were obtained with silicon tips of nominal radius of curvature equal to ~10 nm. For statistical analysis, the root-mean-square (rms) roughness of the *a*-C films was calculated as the mean value of at least four measurements obtained from different AFM images of each film surface. The thickness of each layer comprising the multilayered film structure was measured from cross-sectional HRTEM images.

D. Film Stress Measurement

Film stress measurements were obtained with a Flexus (Tencor FLX-2320) system. A 50-nm-thick *a*-C film was FCVA-deposited on a 4-inch-diamter p-type Si(100) wafer. The residual stress σ in *a*-C films synthesized under different duty cycles of –100 V substrate bias voltage was calculated from Stoney's equation:

$$\sigma = \left(\frac{E}{1-\nu}\right)\frac{h^2}{6Rt} \tag{1}$$

where $E/(1-\nu)$ is the biaxial elastic modulus of the substrate (180.5 GPa for Si(100)), h and t are the thickness of the substrate and the film, respectively, and R is the measured radius of curvature of the substrate.

III. RESULTS AND DISCUSSION

A. Cross-Sectional Film Structure

Fig. 1 shows cross-sectional HRTEM images of *a*-C films for different duty cycles. (The different layers in each multilayer cross-sectional structure are distinguished by white interfaces and are labeled in Fig. 1(d).) The periodic array of the substrate (1) is indicative of the single-crystal structure of Si(100). The structure periodicity decreases close to the substrate interface with the intermixing layer (2) and, eventually, disappears into the film (3), revealing an amorphous structure for both the intermixing layer and carbon film. Structure and contrast differences in the HRTEM images reveal a three-layer structure consisting of crystalline Si(100) substrate, intermixing layer consisting of C, Si, and, possibly, SiC, and *a*-

C film. The Au capping layer (4) and epoxy glue material (5) are also visible in the images. A comparison of the HRTEM images shown in Fig. 1 indicates the formation of significantly thinner *a*-C films for 65% duty cycle (Fig. 1(b)).

B. Film Composition

The overall elemental composition of the *a*-C films shown in Fig. 1 was examined by visible Raman spectroscopy. Because this technique preferentially excites the π states that only exist in sp^2 hybridizations, it can be used to indirectly determine and compare the sp^3 fractions. Fig. 2 shows Raman spectra of *a*-C films for a duty cycle between 50% and 95%. The spectra were fitted with two Gaussian distributions corresponding to the *D* and *G* peaks centered at ~1350 and ~1550 cm^{-1}, respectively. The *D* peak is assigned to the breathing mode of the sp^2 bonds in aromatic rings, whereas the *G* peak is assigned to the stretching mode of all carbon atom pairs in the sp^2 bonds of both aromatic rings and linear chains. Both the position and intensity of the *D* and *G* peaks in visible Raman spectra can be affected by several factors, including sp^2 cluster size, bond-length/angle disorder, and sp^2/sp^3 ratio.

Fig. 3 shows the *G*-peak position and *D*-to-*G* peak intensity ratio $I(D)/I(G)$ versus duty cycle. It is known that the decrease of the sp^3 fraction correlates with the shifting of the *G* peak to higher wavenumbers [40,41]. Fig. 3(a) indicates that the film with the highest sp^3 fraction corresponds to 75% duty cycle. Because the *D* peak indicates the presence of aromatic rings and the *G* peak is mainly due to the vibrations of all sp^2 sites in both chain and ring configurations, the increase in the *D* peak intensity indicates an increase in sp^2 sites [42]. Therefore, the *D*-to-*G* peak intensity ratio can be considered as an index for the indirect comparison of the sp^3 fraction of *a*-C films. Fig. 3(b) shows that the lowest $I(D)/I(G)$ ratio corresponds to 75% duty cycle, suggesting that the *a*-C films deposited under FCVA conditions of 75% duty cycle exhibit an overall higher sp^3 content.

More direct and detailed information about the cross-sectional elemental composition of the *a*-C films can be obtained from analytical EELS, which uses the energy loss of electrons passing through the specimen to determine the chemical composition and structure. Electron energy loss is mainly due to

inelastic electron-electron collisions [43,44]. Beam electrons interacting with electrons of the conduction and/or valence bands of the specimen material are detected in the low-energy loss range (<50 eV) of the EELS spectrum, whereas the high-energy-loss range (>50 eV) yields information about inelastic interactions between beam electrons and inner (core-shell) electrons. Therefore, information about the elemental composition can be extracted from the ionization edges.

Fig. 4 shows high-energy-loss spectra of the C K-edge obtained from different locations across the interface of the Si(100) substrate and an *a*-C film deposited under the FCVA conditions of 75% duty cycle. The location from where each spectrum was obtained is shown in the STEM image on the right of Fig. 4. After performing background subtraction, all spectra were calibrated by centering the π^* peak at 285 eV. As expected, spectrum (a) is featureless because it corresponds to the Si(100) substrate. Spectra (b) and (c) consist of a well-defined π^* peak and a small σ^* peak, indicating the presence of carbon in the intermixing layer. Spectra (d) and (e) correspond to the bulk layer and reveal a high carbon concentration. Spectrum (f) shows a decrease in carbon intensity and an increased contribution of the π^* peak, indicating that the surface layer is rich in sp^2 hybridization. Spectrum (g) corresponds to the Au layer and, therefore, does not show any carbon signal, whereas spectrum (h) contains a strong π^* peak and a relatively weak σ^* peak indicating the existence of carbon and because it corresponds to the epoxy layer.

Fig. 5 shows a representative high-energy-loss spectrum of the C K-edge obtained from the bulk *a*-C film deposited under a duty cycle of 75% and corresponding cross-sectional STEM image on the right. The location from where the spectrum was obtained is marked by a circle in the STEM image. Similar EELS spectra in the range of 280–305 eV were analyzed to determine the sp^2 and sp^3 fractions in the *a*-C film. The pre-edge peak at 285 eV is due to the excitation of electrons from the ground-state 1s core levels to the vacant π^*-like anti-bonding states, while the excitations to the higher lying σ^* states occur above 290 eV [45]. The π^* peak is fitted with a Gaussian distribution, while the σ^* peak is integrated within the small energy window from 290 to 305 eV to minimize plural scattering effects. The

area ratio of these two peaks is proportional to the relative number of π^* and σ^* orbitals, which is 1/3 for 100% sp^2 and 0/4 for 100% sp^3.

The fraction of sp^2 bonded carbon atoms x in the film is given by [45]

$$\frac{(\pi^*/\sigma^*)_{\text{film}}}{(\pi^*/\sigma^*)_{\text{std}}} = \frac{3x}{4-x} \tag{2}$$

where the standard (std) sample is assumed to consist of pure graphite (i.e., 100% sp^2).

Fig. 6 shows the effect of duty cycle of substrate pulse biasing on the normalized intensity obtained by integrating the EELS spectrum from 280 to 305 eV and the depth profiles of sp^3 fraction calculated from the C K-edge spectra using Eq. (2). After performing background subtraction, all C K-edge spectra were calibrated by centering the π^* peak at 285 eV. Regardless of the duty cycle, the sp^3 fraction and carbon concentration reveal the existence of six distinct regions with the following characteristics: (i) *substrate* – the carbon signal intensity is almost zero because this region corresponds to the Si(100) substrate; (ii) *interface layer* – the carbon concentration increases sharply, whereas the sp^3 fraction increases moderately; (iii) *buffer layer* – the further increase of the carbon intensity is accompanied by a sharp increase in sp^3 content, in agreement with previous studies [38,46]; (iv) *bulk film* – the carbon concentration stabilizes at ~100% and the sp^3 fraction is almost constant; (v) *surface layer* – both the carbon concentration and sp^3 fraction decrease sharply; and (vi) *capping layer* – the low intensity of the carbon signal is attributed to carbon from the ambient physisorbed to the surface of the Au capping layer.

Fig. 7 shows the average sp^3 fraction in the bulk layer of the *a*-C film versus duty cycle. The increase of the duty cycle enhances ion bombardment and subplantation, which are conducive to sp^3 hybridization [3]. While the sp^3 content increases with the increase of the duty cycle up to 75% and then tends to slightly decrease. This attributed to thermal spikes due to the excessive C^+ ion bombardment promoted under FCVA deposition conditions of high duty cycle, resulting in relaxation and re-hybridization from sp^3 to sp^2 [3]. The variation of the sp^3 fraction with duty cycle shown in Fig. 7 is consistent with the interpretation of the Raman spectra (Figs. 2 and 3).

C. Thickness

Fig. 8 shows the variation of the thickness of the surface, bulk, buffer, and interface layers (measured from Fig. 6) with the duty cycle. The sum of the thicknesses of all of these layers is referred to as the total thickness. The agreement between TEM and EELS results of the total thickness is fairly good. The minimum total thickness (~10 nm) corresponds to a 65% duty cycle, which is consistent with the HRTEM images (Fig. 1) and EELS results (Fig. 6). Importantly, the 65% duty cycle also produces to the thinnest (~3.6 nm) bulk layer, whereas the 75% duty cycle yields the thickest (~5.3 nm) intermixing layer consisting of a ~2.5-nm-thick interface layer and a ~2.8-nm-thick buffer layer. These results indicate that ion sputtering and subplantation were most effective under FCVA conditions corresponding to a duty cycle of 65% and 75%, respectively.

D. Residual Stress

Further insight into the duty cycle effect on the quality of FCVA-synthesized *a*-C films can be obtained from residual stress measurements. The film stress can be correlated to the dominant hybridization structure. Fig. 9 shows an increasing trend of the residual film stress of *a*-C films versus duty cycles. The compressive residual film stress increases with the increase of the duty cycle up to 75% and then decreases slightly with further increasing the duty cycle. This trend is in good agreement with the variation of the sp^3 fraction in the bulk film (Fig. 7) and previous studies showing a correlation between film residual stress and sp^3 fraction [41,47].

E. Surface Roughness

In addition to the structure and composition, the roughness of the carbon overcoat is also of critical importance because it controls the probability of asperity-asperity interaction at the head-disk interface. Both the intensity and frequency of asperity contact events increase with the film roughness. Fig. 10 shows the rms film roughness as a function of duty cycle. The film roughness increases with the duty cycle increasing above 65% because longer substrate pulse biasing per pulse period enhances C^+ ion-induced sputter etching of the film, whereas for relatively low duty cycle (i.e., 50%) film roughening is

due to the dominance of the deposition process. A balance between sputtering and deposition occurs for a duty cycle of 65%, resulting in minimum film roughness (rms ≈ 0.13 nm), essentially equal to the surface roughness of the Si(100) substrate (rms ≈ 0.12 nm).

The presented results indicate that under FCVA deposition conditions of optimum substrate bias (–100 V) voltage, *a*-C films of minimum thickness, lowest roughness, and predominantly sp^3 hybridized structure are produced for a duty cycle of 65%, attributed to equilibrium of ion-induced sputtering, direct and recoil ion implantation, and deposition. A further decrease in total thickness can be achieved by varying the deposition time and ion incidence angle, which were set at 30 s and 90°, respectively, in the present study, and post-processing Ar^+ ion bombardment of the *a*-C films. For example, the thicknesses of the interface, buffer, and bulk layers can be reduced by increasing the incidence angle of impinging C^+ ions, whereas the sp^2-rich surface layer can be removed by post-deposition Ar^+ ion sputter etching. Results from studies dealing with these effects on the thickness and quality of FCVA-deposited *a*-C films will be presented in a future publication.

IV. Conclusion

The effect of the duty cycle of substrate pulse biasing on the structure, composition, thickness, residual (internal) stress, and surface roughness of FCVA-synthesized *a*-C films was examined in the light of HRTEM, EELS, Raman, film stress, and AFM results. A 65% duty cycle was found to yield smoother and thinner *a*-C films exhibiting relatively high sp^3 content, whereas a 75% duty cycle led to deposition of *a*-C films possessing the highest sp^3 content and residual stress, but also thicker intermixing and buffer layers. These findings reveal a strong duty cycle effect of substrate pulse biasing on carbon atom hybridization and growth, internal stress, and surface roughness of FCVA-synthesized *a*-C films. The results of this study indicate that *a*-C films of thickness only a few nanometers can be deposited under FCVA conditions of 65% duty cycle of –100 V pulse substrate bias voltage. Under the FCVA conditions of optimum duty cycle (i.e., 65%), even thinner *a*-C film can be deposited by modulating other FCVA process parameters, such as incident angle and deposition time.

Acknowledgment

This research was funded by the Computer Mechanics Laboratory (CML), University of California, Berkeley. The TEM/EELS studies were performed at the National Center for Electron Microscope, Lawrence Berkeley National Laboratory, Berkeley (Proposal No. 1886).

References

[1] A. Erdemir and C. Donnet, "Tribology of diamond-like carbon films: recent progress and future prospects," *J. Phys. D: Appl. Phys.*, vol. 39, no. 18, pp. R311–R327, Sept. 2006.

[2] P. K. Chu and L. Li, "Characterization of amorphous and nanocrystalline carbon films," *Mater. Chem. Phys.*, vol. 96, no. 2–3, pp. 253–277, April 2006.

[3] J. Robertson, "Diamond-like amorphous carbon," *Mater. Sci. Eng. R: Reports*, vol. 37, no. 4–6, pp. 129–281, May 2002.

[4] M. H. Kryder, E. C. Gage, T. W. McDaniel, W. A. Challener, R. E. Rottmayer, G. Ju, Y.-T. Hsia, and M. F. Erden, "Heat assisted magnetic recording," *Proc. IEEE*, vol. 96, no. 11, pp. 1810–1835, Nov. 2008.

[5] N. Yasui, H. Inaba, K. Furusawa, M. Saito, and N. Ohtake, "Characterization of head overcoat for 1 Tb/in^2 magnetic recording," *IEEE Trans. Magn.*, vol. 45, no.2 , pp. 805–809, Feb. 2009.

[6] D. R. McKenzie, "Tetrahedral bonding in amorphous carbon," *Rep. Prog. Phys*., vol. 59, no. 12, pp. 1611–1664, Dec. 1996.

[7] O. R. Monteiro, "Thin film synthesis by energetic condensation," *Annu. Rev. Mater. Res*., vol. 31, pp. 111–137, Aug. 2001.

[8] R. L. Wallace, Jr., "The reproduction of magnetically recorded signals," *Bell Syst. Tech. J*., vol. 30, no. 4, pp. 1145–1173, Oct. 1951.

[9] J. Robertson, "Requirements of ultrathin carbon coatings for magnetic storage technology," *Tribol. Int*., vol. 36, no. 4–6, pp. 405–415, April–June 2003.

[10] A. C. Ferrari, "Diamond-like carbon for magnetic storage disks," *Surf. Coat. Technol*., vol. 180–181, pp. 190–206, March 2004.

[11] P. R. Goglia, J. Berkowitz, J. Hoehn, A. Xidis, and L. Stover, "Diamond-like carbon applications in high density hard disc recording heads," *Diam. Relat. Mater*., vol. 10, no. 2, pp. 271–277, Feb. 2001.

[12] C. Casiraghi, A. C. Ferrari, J. Robertson, R. Ohr, M. v. Gradowski, D. Schneider, and H. Hilgers, "Ultra-thin carbon layer for high density magnetic storage devices," *Diam. Relat. Mater*., vol. 13, no. 4–8, pp. 1480–1485, April–Aug. 2004.

[13] M. Zhong, C. Zhang, J. Luo, and X. Lu, "The protective properties of ultra-thin diamond like carbon films for high density magnetic storage devices," *Appl. Surf. Sci*., vol. 256, no. 1, pp. 322–328, Oct. 2009.

[14] C. Casiraghi, A. C. Ferrari, R. Ohr, D. Chu, and J. Robertson, "Surface properties of ultra-thin tetrahedral amorphous carbon films for magnetic storage technology," *Diam. Relat. Mater*., vol. 13, no. 4–8, pp. 1416–1421, April–Aug. 2004.

[15] M. G. Beghi, A. C. Ferrari, K. B. K. Teo, J. Robertson, C. E. Bottani, A. Libassi, and B. K. Tanner, "Bonding and mechanical properties of ultrathin diamond-like carbon films," *Appl. Phys. Lett*., vol. 81, no. 20, pp. 3804–3806, Nov. 2002.

[16] R. Wood, "Future hard disk drive systems," *J. Magn. Magn. Mater*., vol. 321, no. 6, pp. 555–561, March 2009.

[17] Z. Z. Bandić and R. H. Victora, "Advances in magnetic data storage technologies," *Proc. IEEE*, vol. 96, no. 11, pp. 1749–1753, Nov. 2008.

[18] Z.-M. Yuan, B. Liu, T. Zhou, C. K. Goh, C. L. Ong, C. M. Cheong, and L. Wang, "Perspectives of magnetic recording system at 10 Tb/in^2," *IEEE Trans. Magn*., vol. 45, no. 11, pp. 5038–5043, Nov. 2009.

[19] D. S. Grierson, A. V. Sumant, A. R. Konicek, T. A. Friedmann, J. P. Sullivan, and R. W. Carpick, “Thermal stability and rehybridization of carbon bonding in tetrahedral amorphous carbon,” *J. Appl. Phys.*, vol. 107, no. 3, pp. 033523(1)–033523(5), Feb. 2010.

[20] R. Kalish, Y. Lifshitz, K. Nugent, and S. Prawer, “Thermal stability and relaxation in diamond-like-carbon. A Raman study of films with different sp^3 fractions (*ta-C* to *a-C*),” *Appl. Phys. Lett.*, vol. 74, no. 20, pp. 2936–2938, May 1999.

[21] N. Wang and K. Komvopoulos, “Thermal stability of ultrathin amorphous carbon films for energy-assisted magnetic recording,” *IEEE Trans. Magn.*, vol. 47, no. 9, pp. 2277–2282, Sep. 2011.

[22] H.-S. Zhang and K. Komvopoulos, “Direct-current cathodic vacuum arc system with magnetic-field mechanism for plasma stabilization,” *Rev. Sci. Instrum.*, vol. 79, no. 7, pp. 073905(1)–073905(7), July 2008.

[23] G. M. Pharr, D. L. Callahan, S. D. McAdams, T. Y. Tsui, S. Anders, A. Anders, J. W. Ager III, I. G. Brown, C. S. Bhatia, S. R. P. Silva, and J. Robertson, “Hardness, elastic modulus, and structure of very hard carbon films produced by cathodic-arc deposition with substrate pulse biasing,” *Appl. Phys. Lett.*, vol. 68, no. 6, pp. 779–781, Feb. 1996.

[24] I. G. Brown, “Cathodic arc deposition of films,” *Annu. Rev. Mater. Sci.*, vol. 28, pp. 243–269, Aug. 1998.

[25] H.-S. Zhang and K. Komvopoulos, “Synthesis of ultrathin carbon films by direct current filtered cathodic vacuum arc,” *J. Appl. Phys.*, vol. 105, no. 8, pp. 083305(1)–083305(7), April 2009.

[26] J. Zhu, J. Han, X. Han, H. Inaki Schlaberg, and J. Wang, “sp^3-rich deposition conditions and growth mechanism of tetrahedral amorphous carbon films deposited using filtered arc,” *J. Appl. Phys.*, vol. 104, no. 1, pp. 013512(1)–013512(9), July 2008.

[27] N. Wang and K. Komvopoulos, “Incidence angle effect of energetic carbon ions on deposition rate, topography, and structure of ultrathin amorphous carbon films deposited by filtered cathodic vacuum arc,” *IEEE Trans. Magn.*, vol. 48, no. 7, pp. 2220–2227, July 2012.

[28] Y. Wang, H. Li, L. Ji, F. Zhao, X. Liu, Q. Kong, Y. Wang, W. Quan, H. Zhou, and J. Chen, "The effect of duty cycle on the microstructure and properties of graphite-like amorphous carbon films prepared by unbalanced magnetron sputtering," *J. Phys. D: Appl. Phys*., vol. 43, no. 50, pp. 505401, Dec. 2010.

[29] C.-Y. Hsu, L.-Y. Chen, and F. C.-N. Hong, "Properties of diamond-like carbon films deposited by ion plating with a pulsed substrate bias," *Diam. Relat. Mater*., vol. 7, no. 6, pp. 884–891, June 1998.

[30] Z. M. Zeng, X. B. Tian, T. K. Kwok, B. Y. Tang, M. K. Fung, and P. K. Chu, "Effects of plasma excitation power, sample bias, and duty cycle on the structure and surface properties of amorphous carbon thin films fabricated on AISI440 steel by plasma immersion ion implantation," *J. Vac. Sci. Technol. A*, vol. 18, no. 5, pp. 2164–2168, Sept. 2000.

[31] S. Kumar, P. N. Dixit, D. Sarangi, and R. Bhattacharyya, "Possible solution to the problem of high built-up stresses in diamond-like carbon films," *J. Appl. Phys*., vol. 85, no. 7, pp. 3866–3876, April 1999.

[32] S. Anders, A. Anders, I. G. Brown, B. Wei, K. Komvopoulos, J. W. Ager, III, and K. M. Yu, "Effect of vacuum arc deposition parameters on the properties of amorphous carbon thin films," *Surf. Coat. Technol*., vol. 68–69, pp. 388–393, Dec. 1994.

[33] D. Sheeja, B. K. Tay, L. J. Yu, S. P. Lau, J. Y. Sze, and C. K. Cheong, "Effect of frequency and pulse width on the properties of ta:C films prepared by FCVA together with substrate pulse biasing," *Thin Solid Films*, vol. 420–421, pp. 62–69, Dec. 2002.

[34] J.-B. Wu, J.-J. Chang, M.-Y. Li, M.-S. Leu, and A.-K. Li, "Characterization of diamond-like carbon coatings prepared by pulsed bias cathodic vacuum arc deposition," *Thin Solid Films*, vol. 516, no. 2, no. 2–4, pp. 243–247, Dec. 2007.

[35] Y. Lifshitz, S. R. Kasi, J. W. Rabalais, and W. Eckstein, "Subplantation model for film growth from hyperthermal species," *Phys. Rev. B*, vol. 41, no. 15, pp. 10468, May 1990.

[36] M. P. Siegal, P. N. Provencio, D. R. Tallant, R. L. Simpson, B. Kleinsorge, and W. I. Milne, "Bonding topologies in diamondlike amorphous-carbon films," *Appl. Phys. Lett*., vol. 76, no. 15, pp. 2047–2049, April 2000.

[37] C. A. Davis, G. A. J. Amaratunga, and K. M. Knowles, "Growth mechanism and cross-sectional structure of tetrahedral amorphous carbon thin films," *Phys. Rev. Lett*., vol. 80, no. 15, pp. 3280–3283, April 1998.

[38] C. A. Davis, K. M. Knowles, and G. A. J. Amaratunga, "Cross-sectional structure of tetrahedral amorphous carbon thin films," *Surf. Coat. Technol*., vol. 76–77, part 1, pp. 316–321, Nov. 1995.

[39] D. Wan and K. Komvopoulos, "Transmission electron microscopy and electron energy loss spectroscopy analysis of ultrathin amorphous carbon films," *J. Mater. Res*., vol. 19, no. 7, pp. 2131–2136, July 2004.

[40] C. K. Chung, C. C. Peng, B. H. Wu, and T. S. Chen, "Residual stress and hardness behaviors of the two-layer C/Si films," *Surf. Coat. Technol*., vol. 202, no. 4–7, pp. 1149–1153, Dec. 2007.

[41] J.-K. Shin, C. S. Lee, K.-R. Lee, and K. Y. Eun, "Effect of residual stress on the Raman-spectrum analysis of tetrahedral amorphous carbon films," *Appl. Phys. Lett*., vol. 78, no. 5, pp. 631–633, Jan. 2001.

[42] A. C. Ferrari and J. Robertson, "Interpretation of Raman spectra of disordered and amorphous carbon," *Phys. Rev. B*, vol. 61, no. 20, pp. 14095–14107, May 2000.

[43] D. B. Williams and C. B. Carter, *Transmission Electron Microscopy: A Textbook for Materials Science* (Springer, New York, 2009), Ch. 37, pp. 679–681.

[44] R. F. Egerton, *Electron Energy-Loss Spectroscopy in the Electron Microscope* (3rd ed., Springer, New York, 2011), Ch. 3, pp. 111–229.

[45] J. J. Cuomo, J. P. Doyle, J. Bruley, and J. C. Liu, "Sputter deposition of dense diamond-like carbon films at low temperature," *Appl. Phys. Lett*., vol. 58, no. 5, pp. 466–468, Feb. 1991.

[46] N. Wang and K. Komvopoulos, "The multilayered structure of ultrathin amorphous carbon films synthesized by filtered cathodic vacuum arc deposition," *J. Mater. Res.*, vol. 28, no. 16, pp. 2124–2131, Aug. 2013.

[47] J. Robertson, "Diamond-like carbon," *Pure Appl. Chem.*, vol. 66, no. 9, pp. 1789–1796, April 1994.

List of Figures

Fig. 1. Cross-sectional TEM images of *a*-C films for a duty cycle of substrate pulse biasing equal to (a) 50%, (b) 65%, (c) 75%, and (d) 95%. Contrast and structure differences reveal: (1) Si(100) substrate, (2) intermixing layer, (3) bulk film, (4) Au capping layer, and (5) epoxy mounting material.

Fig. 2. Visible Raman spectra of *a*-C films for a duty cycle of substrate pulse biasing between 50% and 95%. For clarity, the spectra have been vertically shifted. The *D*- and *G*-peak positions are shown by dashed lines.

Fig. 3. Visible Raman results of (a) *G*-peak position and (b) *D*-to-*G* peak intensity ratio versus duty cycle of substrate pulse biasing.

Fig. 4. C K-edge EELS spectra obtained from different locations across the interface of the Si(100) substrate and an *a*-C film deposited under conditions of 75% duty cycle of substrate pulse biasing. The locations corresponding to each spectrum are shown in the STEM image on the right. The spectra were calibrated by shifting the π^* peak of all C K-edge spectra to 285 eV after background subtraction.

Fig. 5. C K-edge EELS spectrum of *a*-C bulk film with fitted π^* and σ^* peaks. The location from where the spectrum was obtained is marked by a circle in the STEM image shown on the right. The π^* peak is represented by a Gaussian distribution from 282 to 287.5 eV, whereas the σ^* peak is defined as the spectrum in the energy loss range of 290–305 eV.

Fig. 6. Depth profiles of normalized intensity of C-K edge and sp^3 fraction calculated from C K-edge EELS spectra for a duty cycle of substrate pulse biasing equal to (a) 50%, (b) 65%, (c) 75%, and (d) 95%. Boundaries between neighboring regions are indicated by dashed lines.

Fig. 7. Variation of sp^3 fraction of *a*-C films with duty cycle of substrate pulse biasing.

Fig. 8. Total thickness determined from TEM and EELS analyses and thickness of intermixing, buffer, bulk, and surface layers determined from EELS analysis versus duty cycle of substrate pulse biasing.

Fig. 9. Variation of residual stress of *a*-C films with duty cycle of substrate pulse biasing.

Fig. 10. Root-mean-square surface roughness of *a*-C films versus duty cycle of substrate pulse biasing.

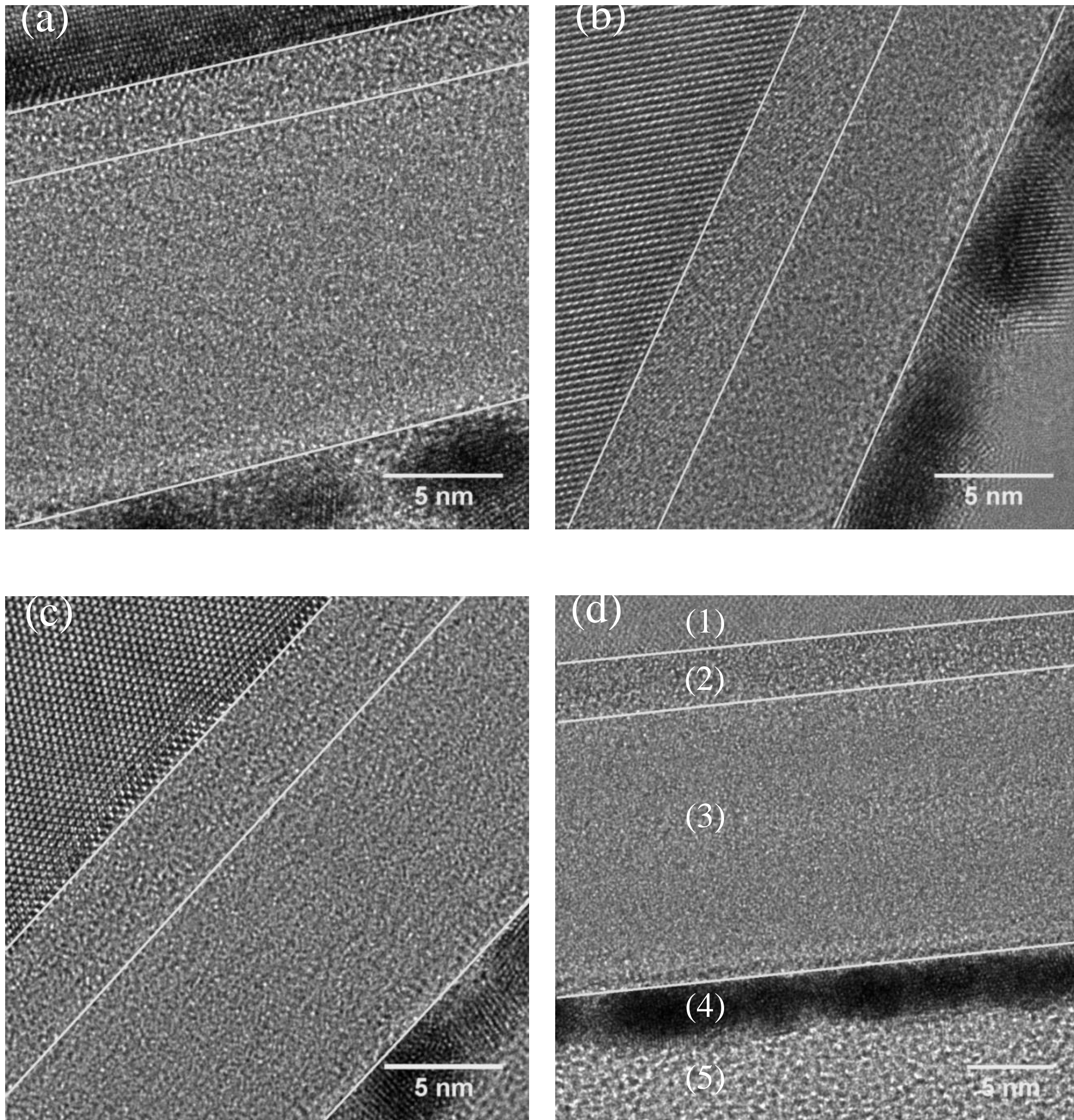

Fig. 1. Cross-sectional TEM images of *a*-C films for a duty cycle of substrate pulse biasing equal to (a) 50%, (b) 65%, (c) 75%, and (d) 95%. Contrast and structure differences reveal: (1) Si(100) substrate, (2) intermixing layer, (3) bulk film, (4) Au capping layer, and (5) epoxy mounting material.

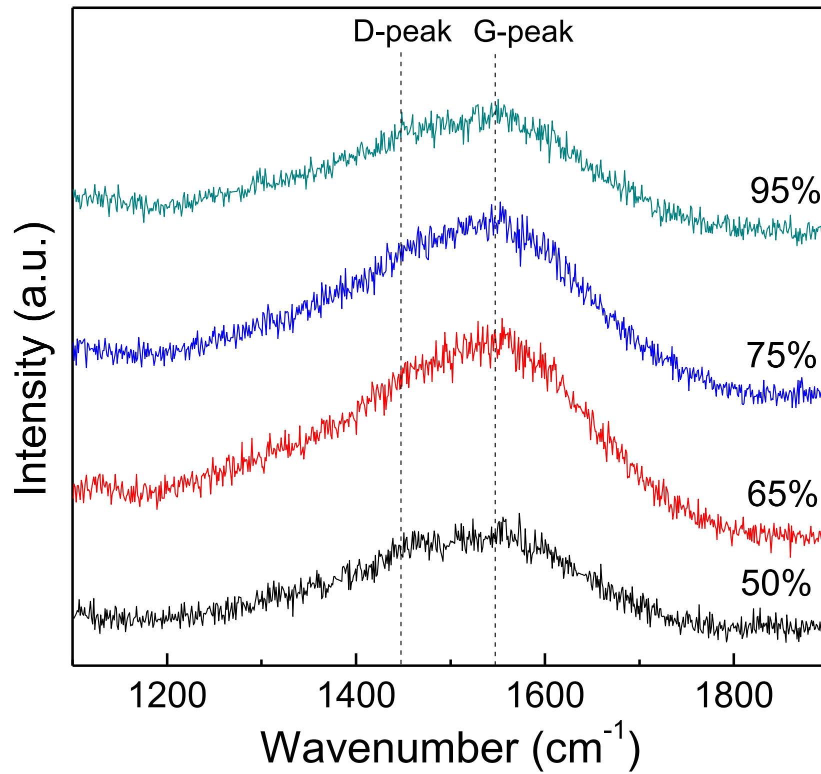

Fig. 2. Visible Raman spectra of *a*-C films for a duty cycle of substrate pulse biasing between 50% and 95%. For clarity, the spectra have been vertically shifted. The *D*- and *G*-peak positions are shown by dashed lines.

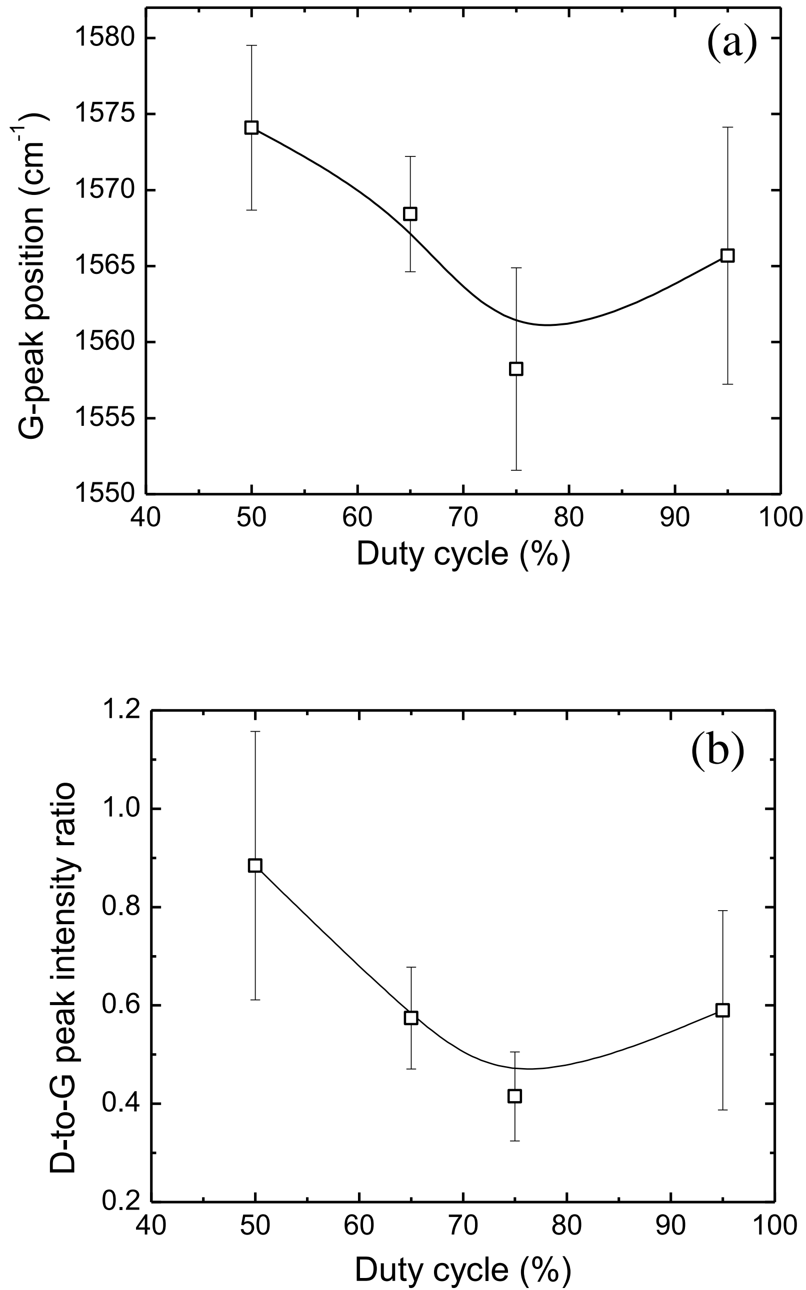

Fig. 3. Visible Raman results of (a) *G*-peak position and (b) *D*-to-*G* peak intensity ratio versus duty cycle of substrate pulse biasing.

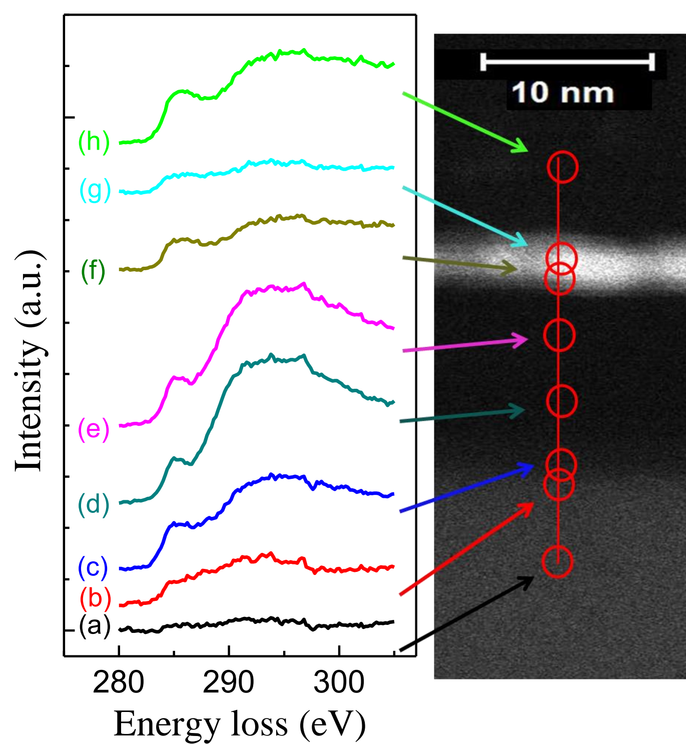

Fig. 4. C K-edge EELS spectra obtained from different locations across the interface of the Si(100) substrate and an *a*-C film deposited under conditions of 75% duty cycle of substrate pulse biasing. The locations corresponding to each spectrum are shown in the STEM image on the right. The spectra were calibrated by shifting the π^* peak of all C K-edge spectra to 285 eV after background subtraction.

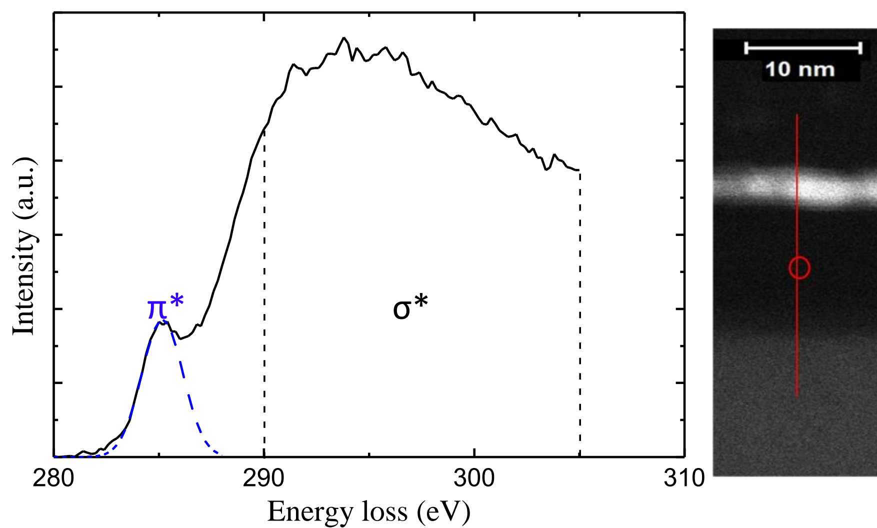

Fig. 5. C K-edge EELS spectrum of *a*-C bulk film with fitted π^* and σ^* peaks. The location from where the spectrum was obtained is marked by a circle in the STEM image shown on the right. The π^* peak is represented by a Gaussian distribution from 282 to 287.5 eV, whereas the σ^* peak is defined as the spectrum in the energy loss range of 290–305 eV.

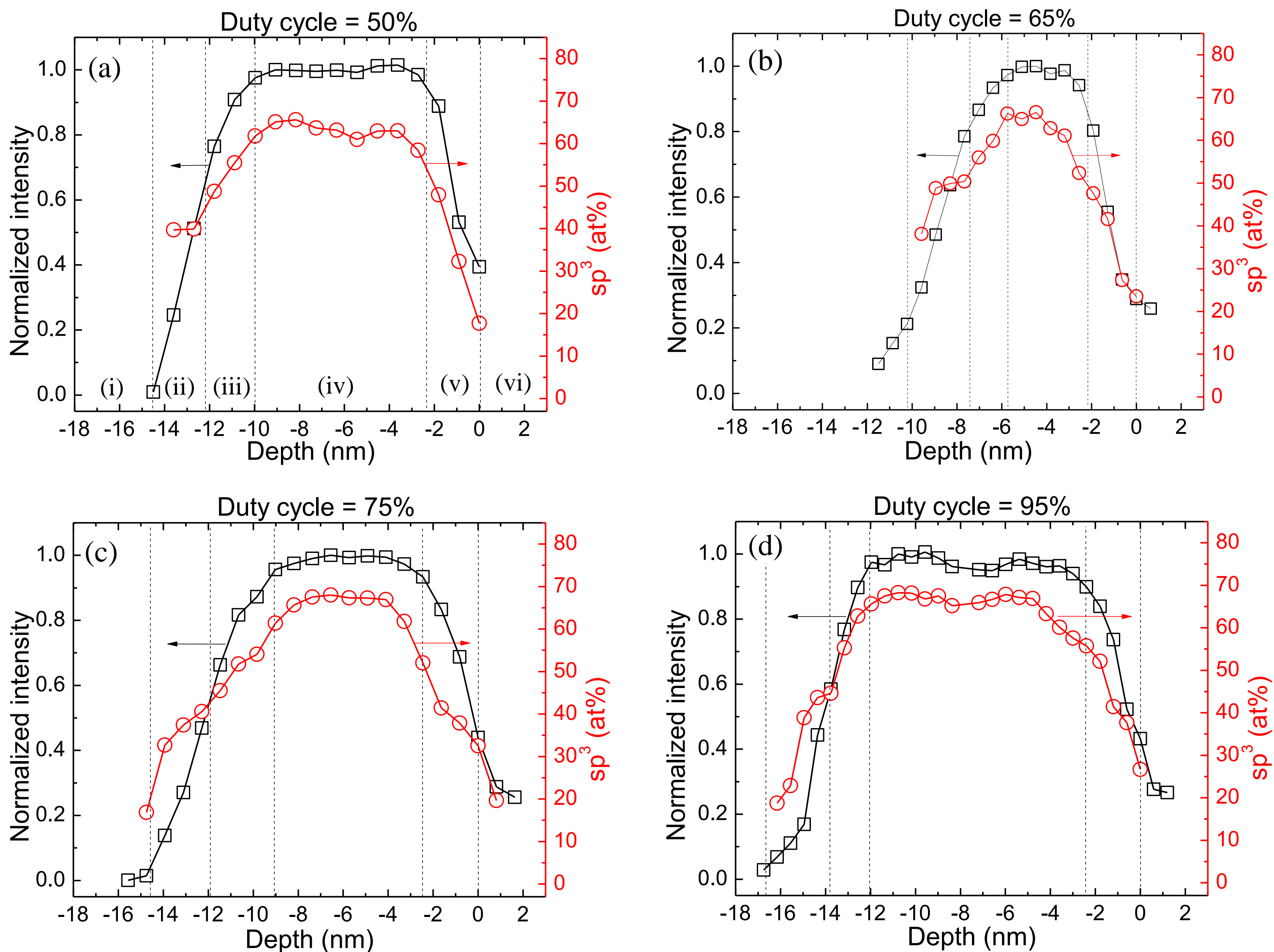

Fig. 6. Depth profiles of normalized intensity of C-K edge and sp^3 fraction calculated from C K-edge EELS spectra for a duty cycle of substrate pulse biasing equal to (a) 50%, (b) 65%, (c) 75%, and (d) 95%. Boundaries between neighboring regions are indicated by dashed lines.

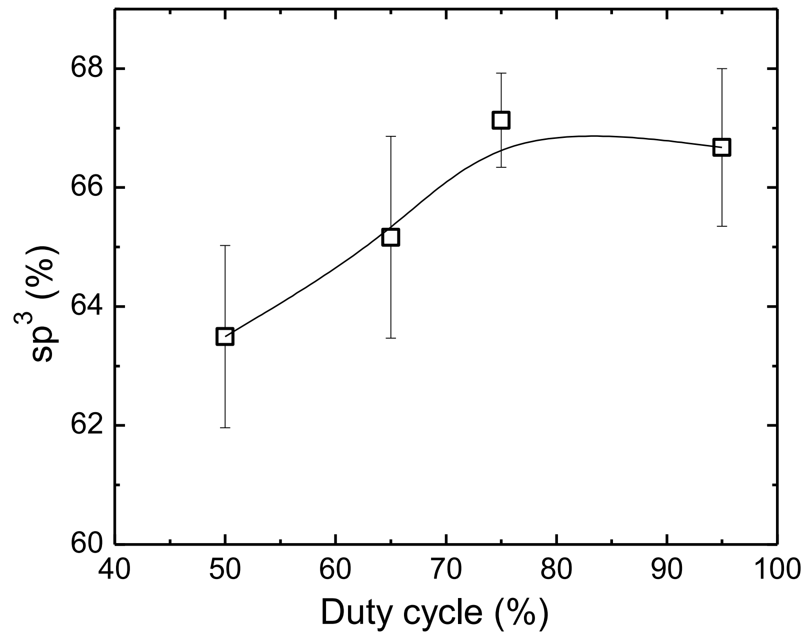

Fig. 7. Variation of sp^3 fraction of *a*-C films with duty cycle of substrate pulse biasing.

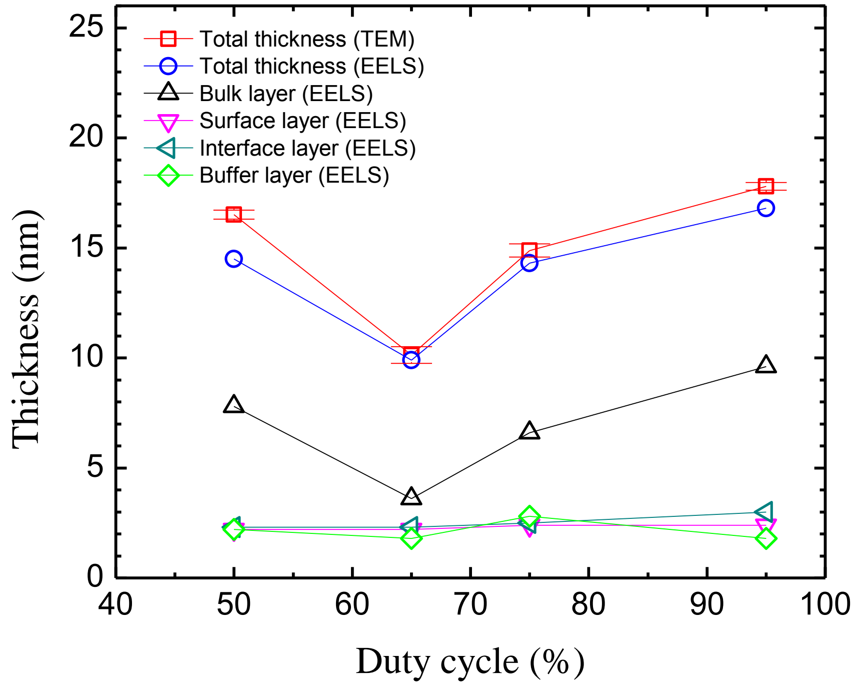

Fig. 8. Total thickness determined from TEM and EELS analyses and thickness of intermixing, buffer, bulk, and surface layers determined from EELS analysis versus duty cycle of substrate pulse biasing.

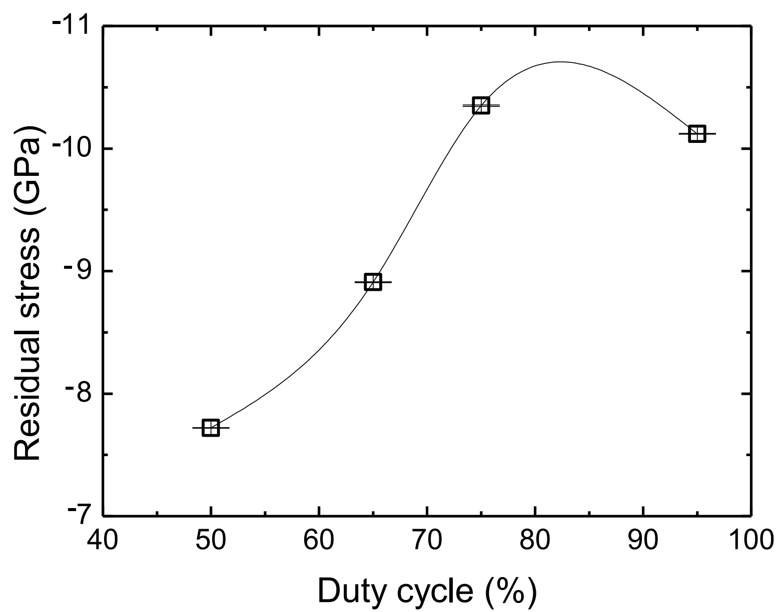

Fig. 9. Variation of residual stress of *a*-C films with duty cycle of substrate pulse biasing.

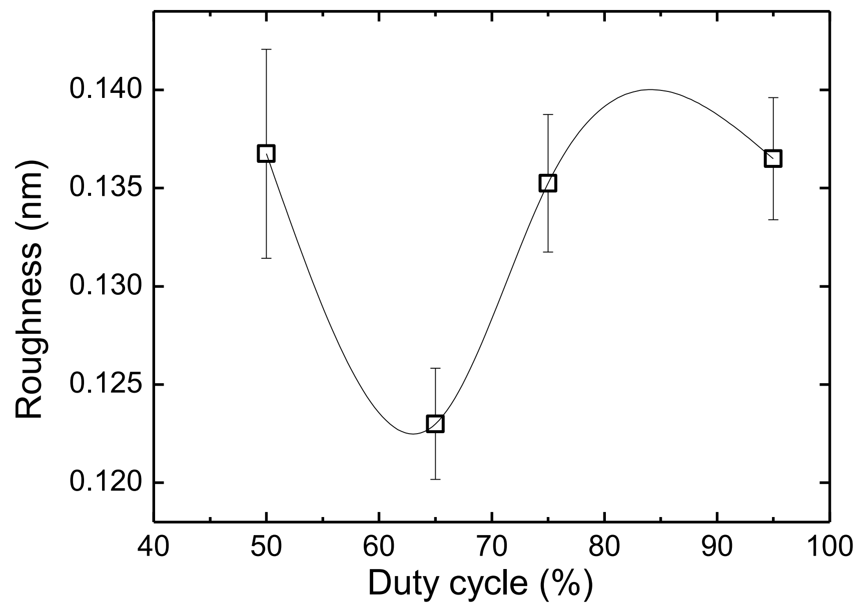

Fig. 10. Root-mean-square surface roughness of *a*-C films versus duty cycle of substrate pulse biasing.